p-ISSN 2089 – 0133 e-ISSN 2477-6416
URL: https://jurnal.uns.ac.id/ijap/article/view/77839

DOI: https://doi.org/10.13057/ijap.v15i1.77839

VISUAL ANALYSIS ON PHOTOACOUSTIC EMISSION IMAGES OF SYNTHETIC DYE CONTRAST AGENTS INSIDE A SIMPLE CLOSED-SURFACE PHANTOM

Mahendra Kusuma Nugraha*[1], Ernawatil Gani[1], Mitrayana[2]
[1]Department of Physics, Faculty of Mathematics and Natural Science, Sam Ratulangi University, Manado, Indonesia
[2]Department of Physics, Faculty of Mathematics and Natural Science, Gadjah Mada University, Yogyakarta, Indoensia
*mahendrakusuma@unsrat.ac.id

Received 13-08-2023, Revised 18-10-2024, Accepted 27-02-2025,
Available Online 01-04-2025, Published Regularly April 2025

ABSTRACT

A straightforward photoacoustic microscopy imaging system utilizing a laser diode emitting photons at wavelength of 450 nanometers was employed for visualizing contrast-enhanced phantom objects. These phantoms consist of polypropylene tubes with a diameter of 0.3 cm, infused with three types of dye solutions: methylene blue, methyl orange, and methyl red, at varying concentrations of 10 ppm, 25 ppm, 50 ppm, and 100 ppm. In total, twelve phantom objects were imaged, each positioned over a 1x1 cm imaging area constructed from composite galvalume plates. A condenser microphone with audiosonic frequency response was employed as the photoacoustic detector, capturing ones generated by the objects. These emissions were subsequently processed and transformed into two-dimensional polychromatic images. Three primary aspects govern the visual characteristics of each acquired image: (i) the visible light absorption capacity at 450 nanometers for each type of dye; (ii) the concentration of soluble dye molecules; and (iii) the geometry and shape of the polypropylene tube functioning as the closed-surface phantom. It was discovered that utilizing polypropylene tubes as the closed-surface phantom can hinder the propagation of photoacoustic emissions generated by the solution, leading to significantly lower measured photoacoustic intensity than expected. When combined with the intrinsic properties of the contrast agents used, this key factor ultimately shapes the image features obtained from this experiment.

Keywords: photoacoustic microscopy; synthetic dye; closed-surface phantom; contrast agent.

Cite this as: Nugraha, M. K., Gani, E., & Mitrayana. 2025. Visual Analysis on Photoacoustic Emission Images of Synthetic Dye Contrast Agents Inside a Simple Closed-Surface Phantom. *IJAP: Indonesian Journal of Applied Physics, 15*(1), 43-58. doi: https://doi.org/10.13057/ijap.v15i1.77839

INTRODUCTION

Photoacoustic microscopy (PAM) is one of two types of photoacoustic imaging systems alongside photoacoustic tomography (PAT) which shares similar fundamentals with thermoacoustic tomography (TAT)[1-3]. Photoacoustic microscopy has emerged as a promising non-ionizing and non-invasive biomedical/clinical imaging technique over the last two decades with dozens of supporting research and improvements[1,3-4]. Photoacoustic imaging modalities like photoacoustic microscopy and photoacoustic tomography have been considered to have the capability to generate detailed biological images with excellent

Copyright © 2025 Universitas Sebelas Maret

spatial resolution, decent to great contrast, and proper penetration/depth range which is useful in surface and sub-surface tissues or even internal organ imaging applications[2-3,5-6].

PAM and PAT can also be utilized to map anatomical structures of surface as well as internal biological tissues/organs with much better spatial resolution—ranging from μm to cm—and deeper penetration up to several centimeters, because photoacoustic emission tends to scatter weaker than photons, resulting in a wider range of sound propagation[4,7]. PAM and PAT are also able to distinguish subtle differences in optical characteristics of many kinds of animals and human tissues[8-10].

Utilization of non-ionizing radiation such as visible light (400-700 nm) and infrared radiation (700-1100 nm)[11-12] also become the main versatility of PAM and PAT. Sources of visible light like LED, PLDs, and semiconductor diodes are considerably cheap, easy to maintain, portable, and simple rather than the bulky class-IV laser system like Nd:YAG[13-14] and OPO[12,15].

The various range of optical and infrared spectrums, each with its own absorption and scattering properties, correspond well with the optical characteristics of wide sorts of biological objects, also known as chromophores which include blood, blood vessel, and even cells[4,6,7,16-17]. Longer wavelengths in infrared spectrums usually result in deeper obtainable images because of the scattering probability that is lower than the one with shorter wavelengths of visible light. However, the significantly lower excitation energy in visible and infrared rays as source radiation compared to standard ionizing ones such as X-ray, may result in images that have a relatively low signal-to-noise ratio (SNR) due to scattering within the surrounding area and other chromophores[14,16,18].

The application of exogenous contrast agents is one of the most achievable optimizations that can be done to increase image quality and sharpen features in PAM/PAT systems[11,19-20]. Synthetic dye is a common type of contrast agent that is highly employed in PAT/PAM systems to emphasize details and visualize biological occurrences through the obtained images[5,11,21-22]. Indocyanine green ($C_{43}H_{47}N_2NaO_6S_2$) [20,23] and methylene blue ($C_{16}H_{18}ClN_3S$) [23-24] are some examples of dyes that are considered effective in optimizing image contrast and detail.

The aim of this experiment is to understand the photoacoustic emission features of methylene blue (MB; $C_{16}H_{18}ClN_3S$), methyl orange (MO; $C_{14}H_{14}N_3NaO_3S$) and methyl red (MR; $C_{15}H_{15}N_3O_2$) dyes with various molecular concentrations that are placed in closed cylindrical phantoms made from polypropylene material. The adoption of a 450 nm visible light radiation source in the PAM system has also become the main underlined parameter, believed to have a detrimental influence on the results.

METHOD

Device and System

The lowkey visible light-based photoacoustic microscopy (PAM) system employed three primary hardware elements. The first one was a semiconductor diode that acted as a 450 nanometers visible laser source with average power level of ~1000 mW. The intensity of the laser could be modulated into determined frequencies by using the TTL logic function available in the system. The goal was to facilitated photoacoustic signal generation from the object/sample.

Copyright © 2025 Universitas Sebelas Maret

The second one was an omnidirectional Behringer® ECM8000 condenser microphone served as the photoacoustic sensor within the audiosonic frequency range. In addition, the data acquisition device which converts and interprets the audiosonic photoacoustic emission into electrical signals was the Behringer® U-PHORIA UMC202 HD sound card. The electrical signals were then transferred into a main processing unit (CPU) to establish two-dimensional images as the representation of photoacoustic signal generated from the object/sample. The last primary component was the Raspberry Pi 4B microcomputer, served as the CPU and to house all other secondary necessary devices with its own software such as ICs and microcontrollers. Assimilation of these hardwares with its corresponding softwares formed the visible light-based photoacoustic microscopy system as mentioned before. Figure 1. shows the system as a whole, which includes the acoustic sensor (microphone), the laser source, and the main processing unit (CPU) along with a monitor to display the Raspberry Pi's interface and other minute components. Figure 2. shows the functional schematic of the system.

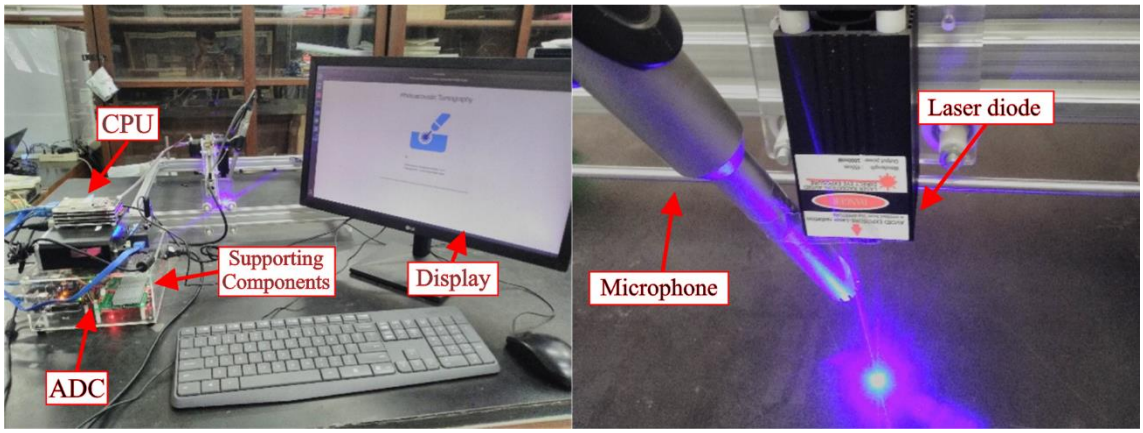

Figure 1. The visible light-based PAM system as a whole, which includes the main processing unit (CPU), the monitor, the ADC hardware and minute components (left). The acoustic sensor (condenser microphone) alongside with the 1000 mW 450 nanometers laser source (right).

The system utilized a standard two-dimensional scanning technique to generate images. This method involves acquiring image pixels continuously from specific points along the horizontal X and Y-axes of the object. The distance between each point or the step size was determined at 0.4 mm. As the scan took place, the transducer moved from the top left to the

Copyright © 2025 Universitas Sebelas Maret

bottom right side of the imaging area, with a delay time of 250 miliseconds between each pixel as illustrated in Figure 3**.**

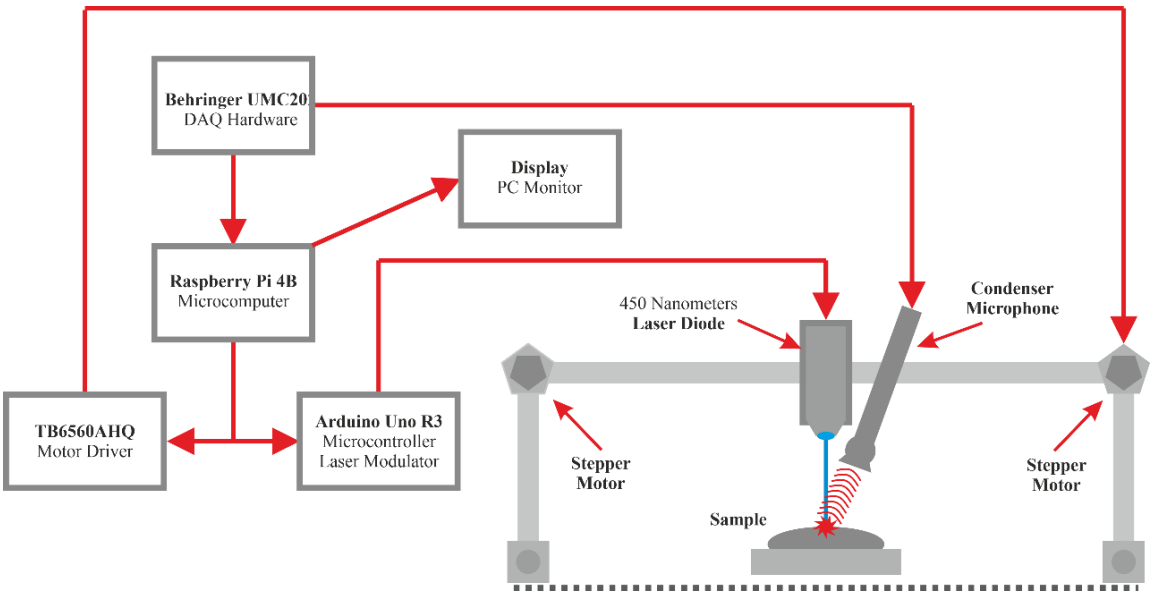

Figure 2. Schematics of the visible light-based PAM system with diagrams of each corresponding component and its function.

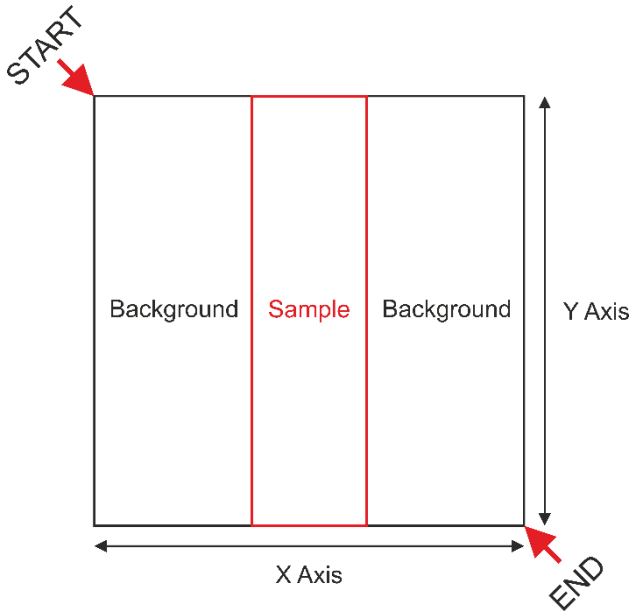

Figure 3. A layout of the two-dimensional image scanning technique, in which the laser source and the microphone travels from the top left point onto the bottom right point.

Dye Syntheses and Phantom Creation

In this stage, the intial dye solutions (5000 ppm for methylene blue and methyl orange, 1000 ppm for methyl red) were thinned out with the appropriate solvent which was distilled water (H_2O). This step was done to achieve different concentration levels for each type of dye solution. The specific concentration value (K_i) for each solution could be calculated using the provided mathematical equation:

$$K_i = \frac{K_0 \times V_0}{(V_i + V_0)} \quad (1)$$

Copyright © 2025 Universitas Sebelas Maret

The K_0 and V_0 parameters corresponded to the initial concentration (ppm) and volume (mL) of the solution, respectively. The term $(V_i + V_0)$ indicated the total volume of the resulting solution after adding the solvent volume (V_i) during the dye dilution process. Figure 4. below shows the the methylene blue, methyl orange, and methyl red dye solutions that have been thinned out into different levels of molecular concentration and stored in separate containers.

Figure 4. The methylene blue (left), methyl orange (middle), and methyl red (right) dye solutions that have been thinned out into different levels of molecular concentration.

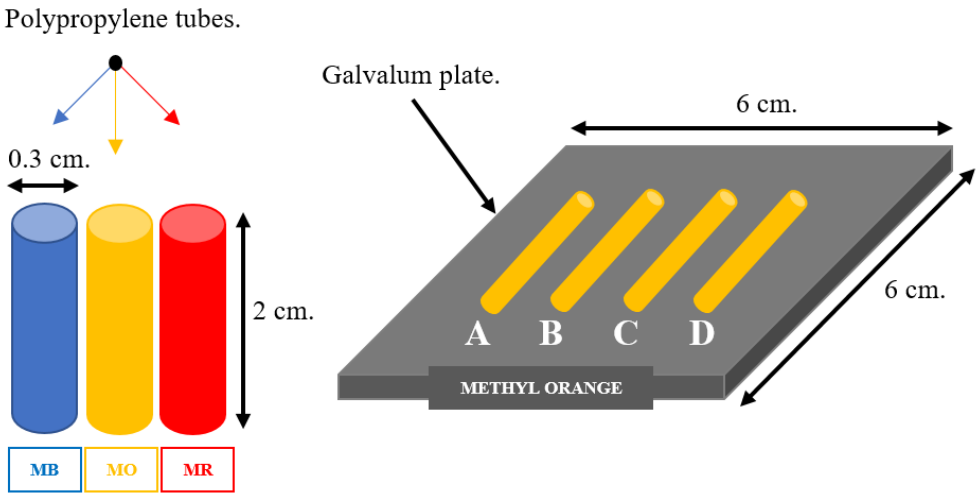

Figure 5. An accurate depiction of the simple photoacoustic imaging phantom using polypropylene tubes filled with methylene blue, methyl orange, and methyl red dye solution.

In the following step, the solutions were diluted to specific concentrations of 10, 25, 50, and 100 ppm. A 1 mL syringe was used to inject these solutions into a 0.3 cm wide polypropylene cylinder that was 2.0 cm in length. During the filling process, it was important to be cautious and prevent any air blockages from occurring inside the tube due to its small size. Once each of the 12 cylinders had been filled with its corresponding solution, they were arranged 10 mm apart from each other in order of their concentration levels on a 6x6 cm coated galvalume plate as illustrated in Figure 5. above.

Amplitude Characterization

Prior to capturing the images, it was crucial to establish the optimal intensity modulation frequency (v_m) and duty cycle percentage $(D_{\%})$ of the laser that was used to image the object. This step was necessary to ensure that the resulting PA images were viable, as the quality of the images was highly reliant on these two specific input parameters.

Copyright © 2025 Universitas Sebelas Maret

To begin with, the phantoms, which consisted of various concentrations of dye solutions, were positioned on the imaging plane. Subsequently, a modulated laser beam was directed at a specific point on the surface of each phantom, using different modulation frequencies (v) that ranged from 15 to 20 kHz, and for a certain duty cycle percentage (30%, 40%, 50%, and 60%) for a specific duration. Afterward, the photoacoustic emissions generated by the object were detected by a condenser microphone positioned at a 70-degree angle relative to the imaging plane.

Furthermore, the photoacoustic signals that were obtained were analyzed by the system's software to represent the level of acoustic intensity (T_I) measured as an arbitrary unit (a.u). that was produced by the photoacoustic effect on each phantom being measured. Subsequently, the average acoustic intensity level obtained from multiple measurements were plotted on a linear scale based on their corresponding modulation frequency values.

Images Acquisition and Analyses

Once the optimal input settings were achieved, the subsequent action was to carry out the phantom imaging, which aimed to assess the system's ability to establish images of three different types of synthetic dye solutions and the polypropylene cylinders that confined them. To conduct this imaging test, a particular 10 by 10 mm region (A) was designated for two-dimensional imaging, and the scanning duration for each pixel (t) was around 250 miliseconds.

The last stage was to perform further examination of the images that were acquired. Initially, this entailed reviewing the pattern detected in the one-dimensional cross-sectional photoacoustic emission amplitude profile of each picture. Additionally, the purpose of this process was to verify the imaging system's ability to precisely represent the object, which was done by comparing the actual object's shape and geometery with the shape of the image that was captured.

RESULT AND DISCUSSION

Power Stability Measurement

The measurement of laser radiation power (P_m) have been included in the previous article within the same research. The analyses conducted indicate that there were no significant variations observed between measured power values during the calibration process for emission stability. Moreover, the standard deviation (σ) values obtained for each input parameter were also quite small. The σ values at an intensity modulation frequency of 10 kHz are 0.0013 (for 50% and 70% duty cycle) and 0.0014 (for 90% duty cycle), respectively. Therefore, it can be concluded that the semiconductor diode utilized as the laser source for this experiment emitted radiation power that was adequately stable.[22]

Visible Absorption Spectrum

The previous work had also conducted absorption spectrum test and analysis on the dyes which showed that the visible-light absorption peak wavelength of 25 ppm of methylene blue was at 651 nm, 25 ppm of methyl orange was at 465 nm, and 25 ppm of methyl red was at 522 nm.[22] From this empirical data, it was known that methyl orange have the closest absorption spectrum range to the 450 nanometers visible-light laser source.

Copyright © 2025 Universitas Sebelas Maret

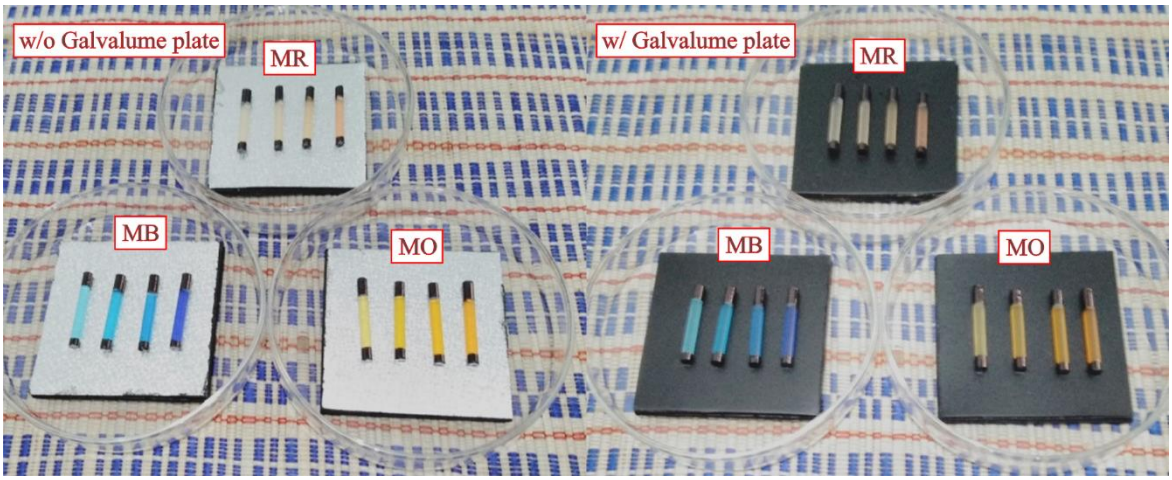

Figure 6. The lowkey polypropylene-based imaging phantom of methylene blue, methyl orange, and methyl red contrast agents with different concentration levels. The phantom sets were laid on top of coated composite aluminium plates, as shown on the right-hand side.

Phantom Preparation

The methylene blue, methyl orange, and methyl red dye solutions which have previously been synthesized into several parts with approximate molecular concentration and have been placed in polypropylene tubes were then arranged on top of 6x6 centimeters composite aluminum plates which was coated with black paint as a background medium. The background medium has to be used in this experiment to clearly distinguish between the photoacoustic signals generated by the solution, by the phantom, or even by the background medium itself. Thus, the resulting photoacoustic image analysis process will be much easier to conduct and apprehend. Figure 6. above shows the arrangement of the phantoms on top of aluminum composite plates as a background medium.

Amplitude Characterization

Following the procedure for characterizing the optimal amplitude of the photoacoustic signal that has been described in the methods section, it was found that the measured acoustic intensity of the 100-ppm methylene blue contrast agent varies non-linearly between 15 kHz and up to 20 kHz modulation frequency (as shown in Figure 7.). This trend is particularly consistent for every duty cycle magnitude ranging from 30% to 60%. It is also known that the average acoustic intensity of the phantom is more strongly affected by an increase in duty cycle magnitude, regardless of changes or variations in the modulation frequency input.

Copyright © 2025 Universitas Sebelas Maret

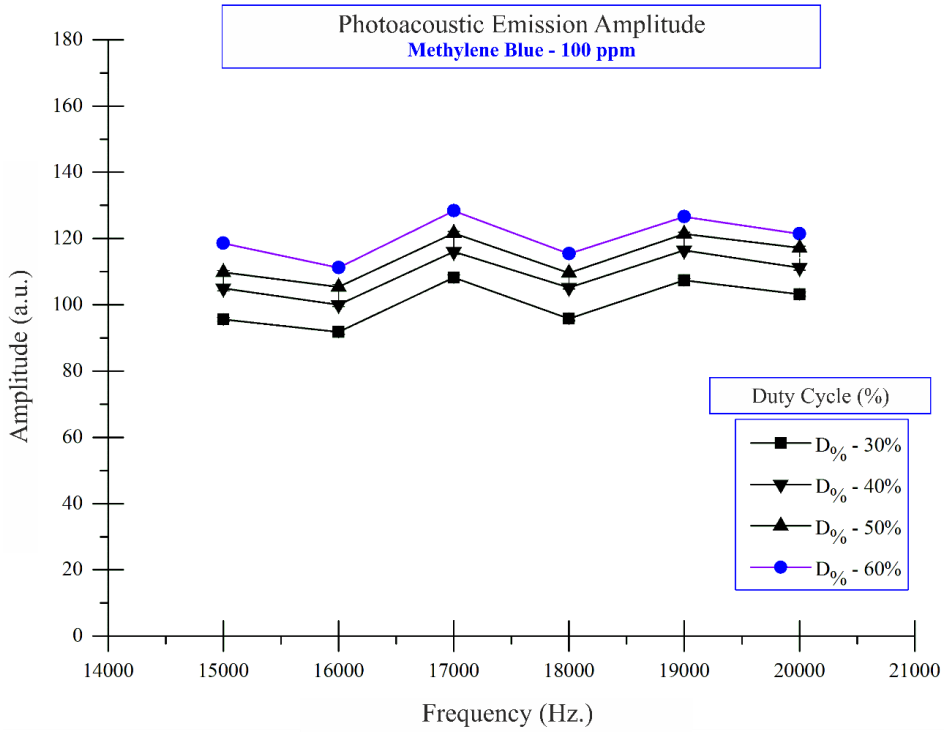

Figure 7. Measured photoacoustic emission amplitude of 100 ppm methylene blue dye solution.

This condition happened due to the proportional relationship between the magnitude of duty cycles and the power of the laser radiation absorbed by the object, which results in a higher level of photoacoustic emission. The two main sources of the photoacoustic signal were the dye solution and the polypropylene phantom. The acoustic signal that came from each of those sources can overlap and interfere with each other. Resulting in total emission measured by the sensor (microphone).

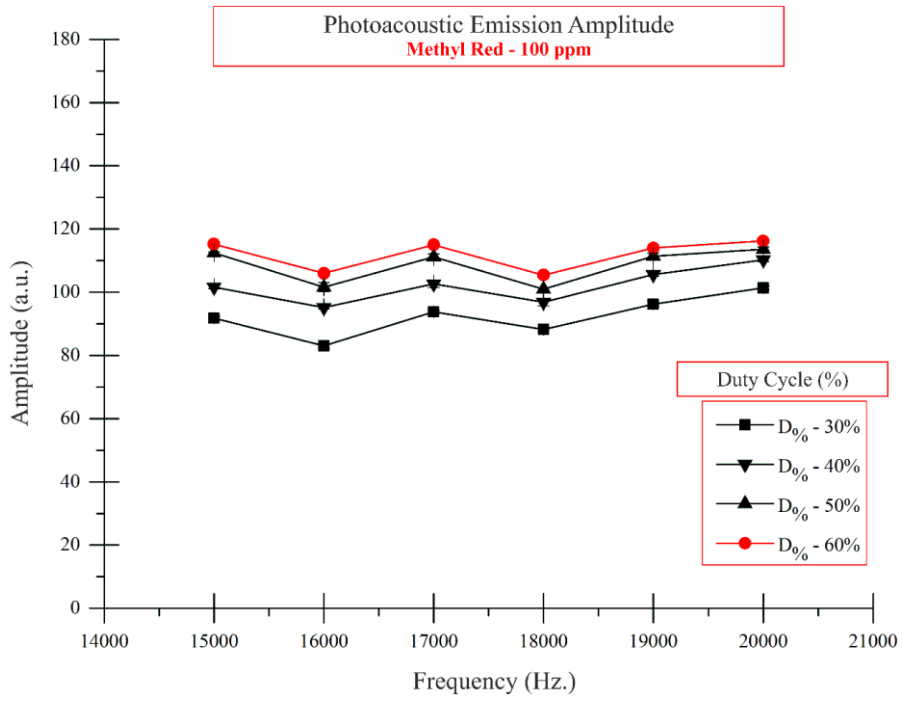

Figure 8. Measured photoacoustic emission amplitude of 100 ppm methyl red dye solution.

Copyright © 2025 Universitas Sebelas Maret

Intensity measurement on the 100-ppm methyl red contrast agent also showed a similar pattern alike the methylene blue (Figure 8.). Although, the overall measured intensities that come from different duty cycles in methyl red phantoms were slightly lower than the overall intensities measured from methylene blue ones. The above condition was surprisingly incoherent knowing the fact that methyl red has a closer visible absorption range ((≅520 nm) with the 450 nanometers laser source than methylene blue ((≅650 nm). Therefore, the resulting average photoacoustic intensity should be greater due to a higher amount of energy being absorbed, but the data contradicted the theoretical basis.

The rather incoherent and enigmatic result above reappears from the results of acoustic intensity measurements on the 100-ppm methyl orange contrast agent which shows a pattern of decreasing emission amplitude along the given input modulation frequency starting from 15 kHz to 20 kHz with its corresponding duty cycle magnitude, as presented in Figure 9. According to the visible absorption spectrum test, it was concluded that methyl orange (≅465 nm) has the closest visible absorption range with the 450 nanometers laser source, which should have contributed to a massively higher measured photoacoustic emission, especially the one that emanated from the dye solution. The obtained experimental data again contradicted the provided theoretical explanation.

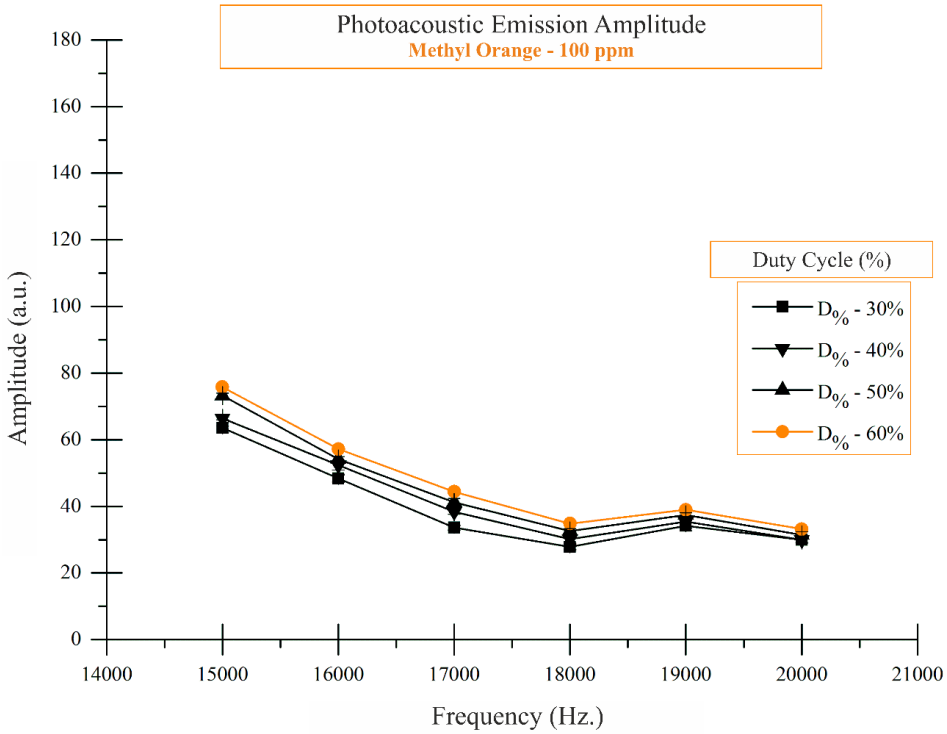

Figure 9. Measured photoacoustic emission amplitude of 100 ppm methyl orange dye solution.

Hence, it was possible that multiple external factors were taken into account to determine the factors responsible for creating such a pattern. The most logical explanation to explain these findings was related to the shape of the polypropylene phantoms that were used. It is hypothesized that the inner wall of the phantom obstructed a large portion of the photoacoustic emission from the dye solution, which prevented it from reaching the sensor. Conversely, the photoacoustic signal generated by the outer wall of the phantom could easily emanate toward the sensor. As a result, the total acoustic intensity measured--which was generated by the dye solution--was considerably lower.

Copyright © 2025 Universitas Sebelas Maret

Therefore, the explanation provides a technical understanding of classifying the composition of the photoacoustic signals that reach the sensor (microphone) based on their sources of emission. For the methylene blue and methyl red phantoms, the majority of the total photoacoustic emission was generated by the outer wall of the polypropylene phantom, as opposed to the dye solution, which tended to reflect a large portion of the 450 nanometers of laser radiation due to its visible absorption property. Contrariwise, in the methyl orange phantom, the largest emission is produced by the methyl orange solution itself. However, because the inner wall of the polypropylene phantom blocked most of the acoustic emission, the total photoacoustic signal that reached the sensor (microphone) was very subtle.

The findings and measurement results obtained above will be validated and confirmed further through visual analysis and interpretation of the phantom images, which are expected to reinforce the explanations described above.

Images Acquisition and Analyses

The number of the lowkey phantoms imaged in this stage were twelve, consisting of four different levels of solute concentration, which were 10, 25, 50, and 100 ppm for each type of dye. The two-dimensional (2D) imaging area was set at 1 by 1 centimeter with a scanning step size of 0.4 millimeters per pixel. The exposure time for a certain pixel was around 250 milliseconds before moving on to the next one. The approximate distance between the sensor (microphone) and the phantom was about 3 centimeters, while the angular position of the sensor relative to the normal plane was 70 degrees. Figure 10**.** shows the photographic top view of the phantoms with the 1×1 centimeter imaging area highlighted in colors.

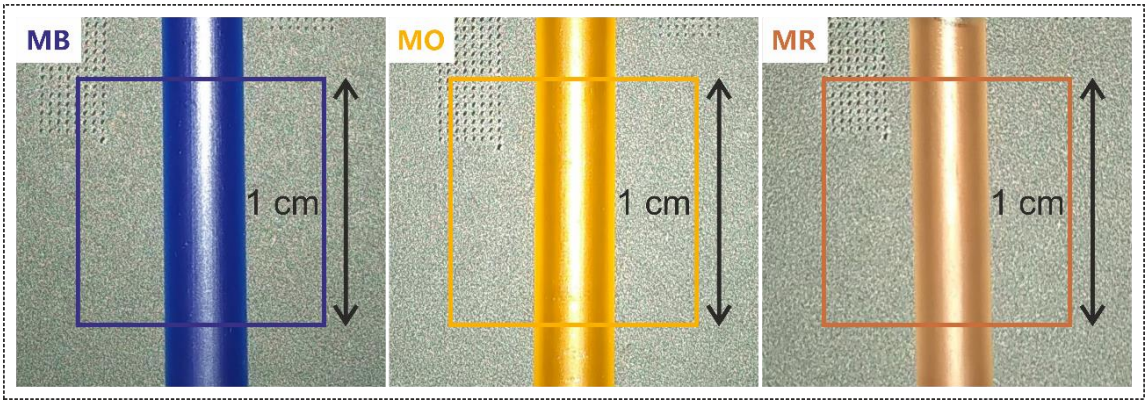

Figure 10. Photographic superior view of the phantoms with the 1×1 centimeter imaging area highlighted in rectangular-shaped colors.

After the image scanning process had finished, the raw pixel data in the form of a CSV file from each of the images was then extracted and represented into a two-dimensional matrix using Visual Studio Code with Python interpreter alongside Numpy and Matplotlib library. The related representations were then mapped into a two-dimensional heatmap with a compatible color profile and a 0.75 σ Gaussian filtration algorithm to obtain images with good contrast and fairly smooth spatial resolution.

Visual analysis performed on the output images of the polypropylene phantoms filled with methylene blue solution with particular concentrations of 10 ppm, 25 ppm, 50 ppm, and 100 ppm--as shown in the Figure 11. revealed that the measured overall photoacoustic emission coming from the phantom and its surrounding environment were quite resemblant to one

Copyright © 2025 Universitas Sebelas Maret

another. The resemblance was pointed out by the hue profile distribution--which represented the magnitude of the photoacoustic emissions--between the phantom and its surroundings that were still enclaved within the same red-yellowish color range. Nevertheless, these obtained images can still be said to have a decent contrast and clarity, noting that the rectangular shape of the polypropylene tube can still be recognized and straightforward to distinguish from the background media around it.

Based on the circumstances above, the central source of the photoacoustic emission produced by the phantom part was believed to be originated from the outer wall of the enclosing polypropylene tube rather than from the methylene blue solution itself inside it due to methylene blue's tendency to scatter and reflect the 450 nanometers wavelength emanating from the laser diode. Nonetheless, if there was even a small magnitude of photoacoustic emission produced by the solution inside the tube, certainly be assured that the inner wall of the polypropylene tube has blocked that small quantity from reaching the transducer.

Before delving into the subsequent discussion and drawing further conclusions, it was evident that the utilization of transparent polypropylene tubes as enclosed containers for methylene blue solutions significantly impacted the characteristics and visual aspects of the resulting images.

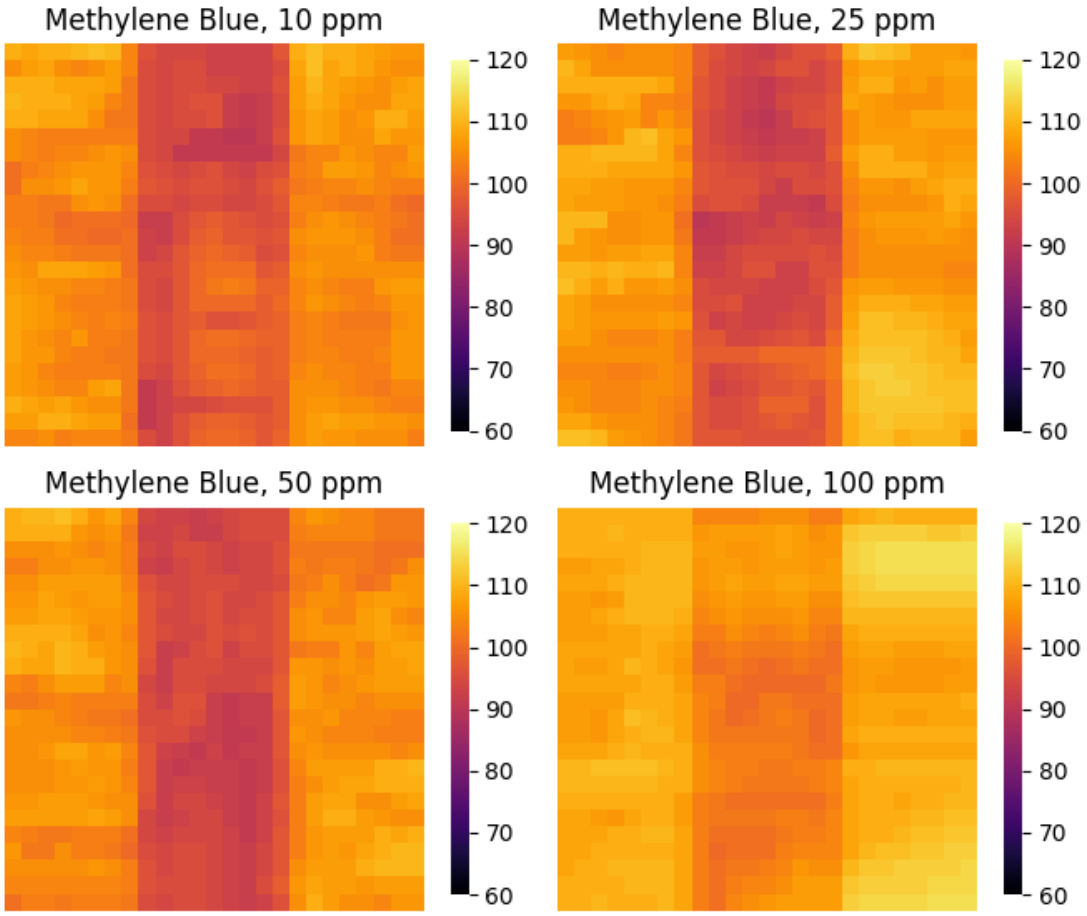

Figure 11. Polychromatic images of polypropilene tubes infused with different concentration of methylene blue solutions.

Copyright © 2025 Universitas Sebelas Maret

A parallel visual analysis was also conducted on images of polypropylene tubes containing solutions of methyl orange and methyl red at identical concentrations: 10 ppm, 25 ppm, 50 ppm, and 100 ppm. As depicted in Figure 12 and 13, the striking distinction between these images and those of polypropylene tubes containing methylene blue solutions is immediately apparent.

Notably, the polypropylene tubes, housing both methyl orange and methyl red solutions, stand out prominently at the center of the objects. They are conspicuously discernible from the surrounding background medium due to their markedly darker pixel intensity compared to the pixels comprising the backdrop. The emergence of these distinct chromatic features is attributed to the measured photoacoustic emission profiles, obtained through microphones at each pixel locus constituting the whole image. The accompanying color scale corroborates that the measured photoacoustic emission intensity originating from the core of the object (polypropylene tube) tends to be lower than the emissions generated by the background medium (galvalume plate). The blackish-blue color profile indicates that the measured photoacoustic emission intensity is lower than the yellowish-red color profile.

This observation is decidedly unconventional, given that methyl orange, when in solution, exhibits a substantial capacity for absorbing visible light at a wavelength of 450 nanometers. This intriguing fact could potentially serve as a pivotal empirical reference, implying that polypropylene tubes containing specifically 100 ppm concentration of methyl orange ought to manifest a notably substantial photoacoustic amplitude.

The reciprocal explanations that can be further elucidated from this discovery are primarily twofold. Firstly, it was indeed established that a significant portion of photon energy originates from the 450-nanometer laser, which was absorbed seamlessly by the solution without encountering any notable transmission disruptions. This phenomenon was due to the transparent physical attributes of the polypropylene tube. However, the photoacoustic emissions generated by the object—stemming from the creation of pressure waves resulting from periodic molecular vibrations—are hindered from propagating outward through the inner walls of the polypropylene tube. Consequently, they tend to gradually attenuate over time, transforming into heat through the phenomenon of vibrational propagation around the inner wall onto the outer wall. As a result, the aforementioned photoacoustic emissions fail to reach the transducer microphone at their maximum amplitude, leading to a minimal measurable emission intensity.

Copyright © 2025 Universitas Sebelas Maret

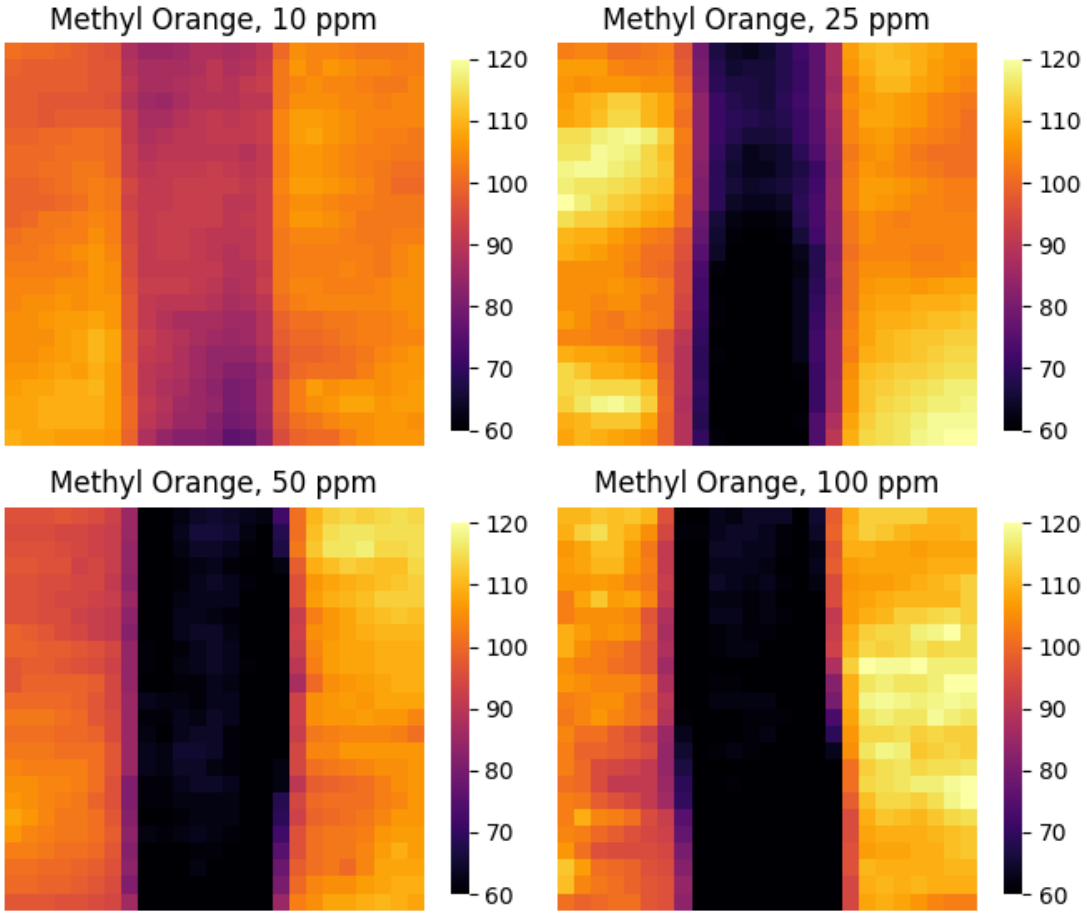

Figure 12. Polychromatic images of polypropilene tubes infused with different concentration of methyl orange solutions.

This finding was also previously identified during the stage of measuring emission amplitude, depicted in Figure 9. On the other hand, the acoustic emissions generated by the background medium can effortlessly propagate directly through the free air towards the microphone, yielding a significantly more impactful amplitude acquisition. Ultimately, this circumstance becomes the rationale behind the observable visual features, particularly evident in the images of polypropylene tubes containing methyl orange solutions.

It can also be observed that variations in the concentration of the solution have an impact on the visual features of the acquired images. In this case, the polypropylene tube containing 100 ppm methyl orange solution actually yields significantly lower emissions compared to the one containing 10 ppm methyl orange solution. Theoretically, the light absorption capacity at visible wavelength of 450 nanometers possessed by the 10 ppm methyl orange solution is certainly lower than that of the 100 ppm methyl orange solution, thus indicating a higher tendency for scattering that resulted in reduction of the probability of photoacoustic effects occurring. Therefore, it can be surmised that the overall measured photoacoustic emission composition captured by the microphone does not solely originate from the respective solution, but rather from the outer walls of the polypropylene tube, as evidenced in the images of polypropylene tubes containing methylene blue solutions in Figure 11.

Copyright © 2025 Universitas Sebelas Maret

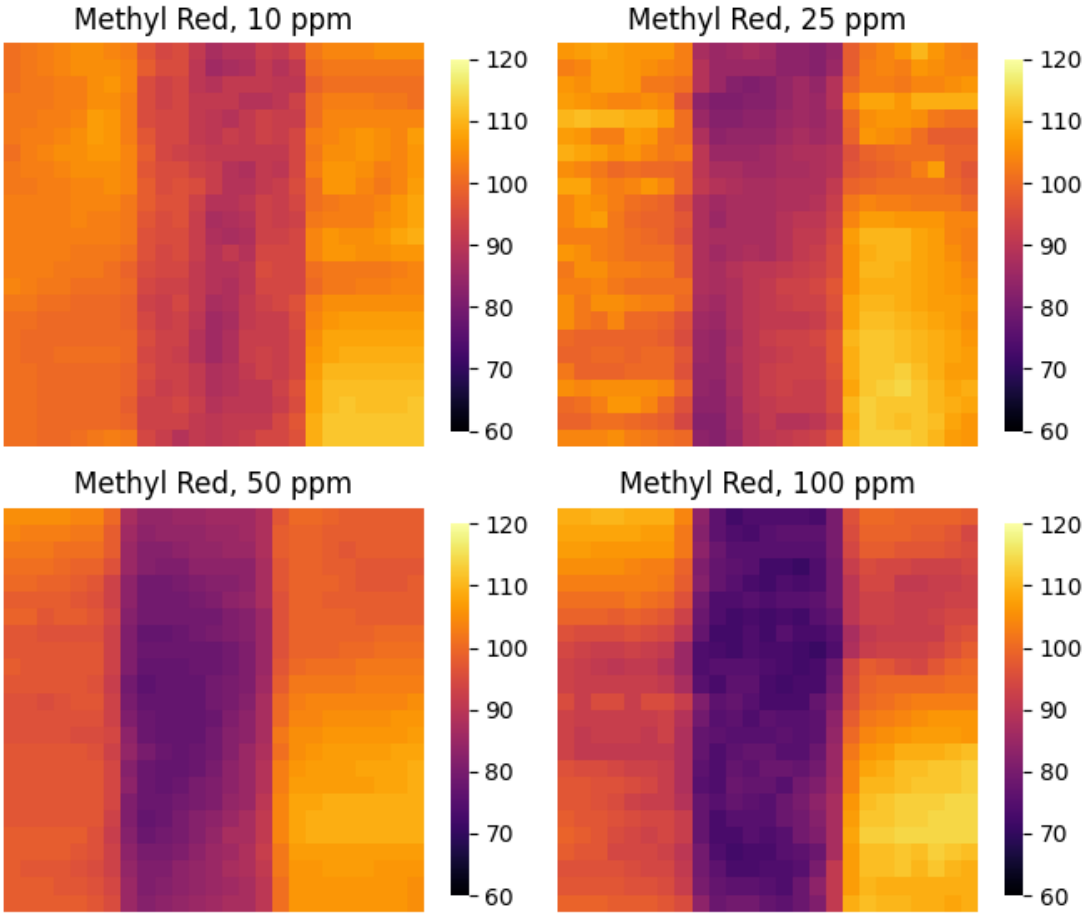

Figure 13. Polychromatic images of polypropilene tubes infused with different concentration of methyl red solutions.

Slight variations in color profiles and contrast can also be observed between the images of polypropylene tubes containing methyl red and those containing methyl orange solutions, which are essentially found in the amplitude of the total measured photoacoustic emissions captured by the microphone. Ultimately, this discrepancy affects the visual features that emerge in each image. The methyl red solution has a lower capacity to absorb light at the 450-nanometer wavelength compared to the methyl orange solution but higher than the methylene blue solution. The appearance of color profiles in the images of polypropylene tubes containing a 100 ppm methyl red solution can be described as brighter than the images of polypropylene tubes containing a 100 ppm methyl orange solution, yet darker than the images of polypropylene tubes containing a 10 ppm methylene blue solution. These characteristics align with the scientific explanations presented in previous discussions, where the presence of the polypropylene tube used as an enclosed container for each dye solution significantly influences the characteristics of the acquired images.

CONCLUSION

Based on the extensive explanations provided above, the following conclusions can be drawn. It has been discovered that the photon light absorption capacity evident in various types of dye solutions does not solely and directly influence the visual attributes and characteristics of the resulting images. Another significant factor at play is the presence of the polypropylene tube itself. It's important to understand that the color profile formed

Copyright © 2025 Universitas Sebelas Maret

within each image serves as a visual-quantitative representation of the photoacoustic emissions measured by microphones at each pixel composing the entire image. In this context, the reddish-yellow color spectrum signifies high measured emission intensity, while the bluish-dark spectrum represents low measured emission intensity.

It is strongly believed that the inner walls of the polypropylene tube interfere with the transmission of the generated acoustic waves (primary emissions) originating from the dye solution as they propagate towards the microphone. Nevertheless, interactions involving photon energy absorption and photoacoustic effects also occur at the outer walls of the tube, leading to the creation of secondary photoacoustic emission sources. These primary and secondary emissions overlap and directly assimilate to form the color profile and visual features of the images obtained from each object and specified variation. Up to this point, there have been three primary factors and key aspects influencing the visual features and characteristics of each acquired image. These are: (i) the visible light absorption capacity at 450 nanometers for each type of dye solution; (ii) the concentration of soluble dye molecules; and (iii) the geometry and physical shape of the polypropylene tube functioning as the closed-surface phantom.

One approach to address this irregularity is to identify a material for the phantom that does not produce the same inconsistencies observed in this experiment. This would enable more accurate readings and analyses of the intrinsic properties of the dye solution when subjected to similar treatment. This discovery serves as a crucial lesson and enhances the understanding pertaining to the utilization and application of phantom objects with closed-container geometric configurations, especially in the realm of visible light-based photoacoustic microscopy techniques.

ACKNOWLEDGEMENTS

The corresponding author received plenty of helpful assistance from the tendance staff at the Atomic and Nuclear Laboratory, Physics Department, Faculty of Mathematics and Natural Sciences, Gadjah Mada University, for the entire duration of the research. Therefore, the authors express their most gratitude and respect towards the staff for their support.

REFERENCES

1 Zhou, Y., Yao, J., & Wang, L. V. 2016. Tutorial on photoacoustic tomography. *Journal of Biomedical Optics*, *21*(6), 061007.

2 Deng, H., Qiao, H., Dai, Q., & Ma, C. 2021. Deep learning in photoacoustic imaging: a review. *Journal of Biomedical Optics*, *26*(04), 1–32.

3 Wang, L. V., & Yao, J. 2016. A practical guide to photoacoustic tomography in the life sciences. *Nature Methods*, *13*(8), 627–638.

4 Hysi, E., Moore, M. J., Strohm, E. M., & Kolios, M. C. 2021. A tutorial in photoacoustic microscopy and tomography signal processing methods. *Journal of Applied Physics*, *129*(14).

5 Kim, C., Erpelding, T. N., Jankovic, L., & Wang, L. V. 2011. Performance benchmarks of an array-based hand-held photoacoustic probe adapted from a clinical ultrasound system for non-invasive sentinel lymph node imaging. *Philosophical Transactions of the Royal Society A: Mathematical, Physical and Engineering Sciences*, *369*(1955), 4644–4650.

6 Jeon, S., Kim, J., Lee, D., Baik, J. W., & Kim, C. 2019. Review on practical photoacoustic microscopy. *Photoacoustics*, *15*(July), 100141. https://doi.org/10.1016/j.pacs.2019.100141

7 Liu, W. W., & Li, P. C. (2020). Photoacoustic imaging of cells in a three-dimensional microenvironment. *Journal of Biomedical Science*, *27*(1), 1–9.

Copyright © 2025 Universitas Sebelas Maret

8 Hosseinaee, Z., Tummon Simmons, J. A., & Reza, P. H. 2021. Dual-Modal Photoacoustic Imaging and Optical Coherence Tomography [Review]. *Frontiers in Physics*, *8*(January), 1–19.
9 Attia, A. B. E., Balasundaram, G., Moothanchery, M., Dinish, U. S., Bi, R., Ntziachristos, V., & Olivo, M. 2019. A review of clinical photoacoustic imaging: Current and future trends. *Photoacoustics*, *16*(November), 100144.
10 Steinberg, I., Huland, D. M., Vermesh, O., Frostig, H. E., Tummers, W. S., & Gambhir, S. S. (2019). Photoacoustic clinical imaging. *Photoacoustics*, *14*(June), 77–98.
11 Weber, J., Beard, P. C., & Bohndiek, S. E. 2016. Contrast agents for molecular photoacoustic imaging. *Nature Methods*, *13*(8), 639–650.
12 Jung, U., Ryu, J., & Choi, H. 2022. Optical Light Sources and Wavelengths within the Visible and Near-Infrared Range Using Photoacoustic Effects for Biomedical Applications. *Biosensors*, *12*(12).
13 Zhong, H., Duan, T., Lan, H., Zhou, M., & Gao, F. 2018. Review of Low-Cost Photoacoustic Sensing and Imaging Based on Laser Diode and Light-Emitting Diode. *Sensors MDPI*, *18*(2264), 1–24.
14 Zhu, Y., Xu, G., Yuan, J., Jo, J., Gandikota, G., Demirci, H., Agano, T., Sato, N., Shigeta, Y., & Wang, X. 2018. Light emitting diodes based photoacoustic imaging and potential clinical applications. *Scientific Reports*, *8*(1), 1–12.
15 Kalva, S. K., Upputuri, P. K., Rajendran, P., Dienzo, R. A., & Pramanik, M. 2019. Pulsed Laser Diode-Based Desktop Photoacoustic Tomography for Monitoring Wash-In and Wash-Out of Dye in Rat Cortical Vasculature. *Journal of Visualized Experiments*, *147*(May), 1–6.
16 Kim, J., Kim, J. Y., Jeon, S., Baik, J. W., Cho, S. H., & Kim, C. 2019. Super-resolution localization photoacoustic microscopy using intrinsic red blood cells as contrast absorbers. *Light: Science & Applications*, *8*(103), 1–11.
17 Lan, B., Liu, W., Wang, Y., Shi, J., Li, Y., Xu, S., Sheng, H., Zhou, Q., Zou, J., Hoffmann, U., Yang, W., & Yao, J. 2018. High-speed widefield photoacoustic microscopy of small-animal hemodynamics. *Biomedical Optics Express*, *9*(10), 4689.
18 Erfanzadeh, M., & Zhu, Q. 2019. Photoacoustic imaging with low-cost sources; A review. *Photoacoustics*, *14*(January), 1–11.
19 Wu, D., Huang, L., Jiang, M. S., & Jiang, H. 2014. Contrast Agents for Photoacoustic and Thermoacoustic Imaging: A Review. *International Journal of Molecular Sciences*, *15*(12), 23616–23639.
20 Capozza, M., Blasi, F., Valbusa, G., Oliva, P., Cabella, C., Buonsanti, F., Cordaro, A., Pizzuto, L., Maiocchi, A., & Poggi, L. 2018. Photoacoustic imaging of integrin-overexpressing tumors using a novel ICG-based contrast agent in mice. *Photoacoustics*, *11*(August), 36–45.
21 Gao, F., Kishor, R., Feng, X., Liu, S., Ding, R., Zhang, R., & Zheng, Y. 2017. An analytical study of photoacoustic and thermoacoustic generation efficiency towards contrast agent and film design optimization. *Photoacoustics*, *7*(May), 1–11.
22 Nugraha, M. K., Wasono, M. A. J., & Mitrayana, M. 2022. Performance Characterization of 450 nm Visible Light Based Photoacoustic Imaging for Phantom Imaging of Synthetic Dye Contrast Agents. *Indonesian Journal of Applied Physics*, *12*(1), 124.
23 Hariri, A., Lemaster, J., Wang, J., Jeevarathinam, A. K. S., Chao, D. L., & Jokerst, J. V. 2018. The characterization of an economic and portable LED-based photoacoustic imaging system to facilitate molecular imaging. *Photoacoustics*, *9*(November), 10–20.
24 Arconada-Alvarez, S. J., Lemaster, J. E., Wang, J., & Jokerst, J. V. 2017. The development and characterization of a novel yet simple 3D printed tool to facilitate phantom imaging of photoacoustic contrast agents. *Photoacoustics*, *5*(February), 17–24.

Copyright © 2025 Universitas Sebelas Maret